Iwaki *et al. Earth, Planets and Space* (2016) 68:95
DOI 10.1186/s40623-016-0473-6

Earth, Planets and Space

FULL PAPER Open Access

# Kinematic source models for long-period ground motion simulations of megathrust earthquakes: validation against ground motion data for the 2003 Tokachi-oki earthquake

Asako Iwaki*, Takahiro Maeda, Nobuyuki Morikawa, Shin Aoi and Hiroyuki Fujiwara

**Abstract**

In this study, a method for simulating the ground motion of megathrust earthquakes at periods of approximately 2 s and longer was validated by using the characterized source model combined with multi-scale spatial heterogeneity. Source models for the $M_W$ 8.3, 2003 Tokachi-oki earthquake were constructed, and ground motion simulations were conducted to test their performance. First, a characterized source model was generated based on a source model obtained from waveform inversion analysis. Then, multi-scale heterogeneity was added to the spatial distribution of several source parameters to yield a heterogeneous source model. An investigation of the Fourier spectra and 5 % damped velocity response spectra of the simulated and observed ground motions demonstrated that adding multi-scale heterogeneity to the spatial distributions of the slip, rupture velocity, and rake angle of the characterized source model is an effective method for constructing a source model that explains the ground motion at periods of 2–20 s. It was also revealed how the complexity of the parameters affects the resulting ground motion. The complexity of the rupture velocity had the largest influence among the three parameters.

**Keywords:** Long-period ground motion, 2003 Tokachi-oki earthquake, Characterized source model, Multi-scale heterogeneity

## Introduction

Megathrust ($M_W > 8$) earthquakes have occurred and will potentially occur in the vicinity of the islands of Japan, including along the Kurile Trench, the Japan Trench, the Sagami Trough, the Nankai Trough, and the Ryukyu Trench. Past megathrust earthquakes have repeatedly brought strong ground motion to land areas; thus, seismic hazard evaluation for future megathrust earthquakes is an urgent issue today. In particular, long-period components of ground motion are expected to be significantly amplified in distant sedimentary basins during future megathrust earthquakes, as observed in recent earthquakes such as the 1985 Michoacan earthquake (e.g., Anderson et al. 1986) and the 2003 Tokachi-oki earthquake (e.g., Koketsu et al. 2005). During the 2011 M9 Tohoku earthquake, the velocity response spectra observed in the Osaka sedimentary basin, approximately 600 km from the source area, exceeded 50 cm/s at periods of 6–7 s (Sato et al. 2012), which caused damages to elevators and non-structural elements of high-rise buildings.

In general, long-period components of ground motion are computed using a deterministic approach with a theoretical representation of the rupture and wave propagation processes; therefore, it is important to construct an appropriate source model and a three-dimensional (3D) velocity structure model. 3D long-period ground motion simulations for future megathrust earthquakes have been presented by numerous works (e.g., Olsen et al. 2008; Pulido et al. 2015). The authors recently studied long-period ground motions for future events at the Nankai and the Sagami Troughs, with the goal of performing

*Correspondence: iwaki@bosai.go.jp
National Research Institute for Earth Science and Disaster Resilience, 3-1 Tennodai, Tsukuba, Ibaraki 305-0006, Japan

seismic hazard evaluation considering the uncertainties of the source parameters (Maeda et al. 2013; Iwaki et al. 2013). These simulations used the 3D Japan integrated velocity structure model (JIVSM; Koketsu et al. 2009) and kinematic source models based on the concept of characterized source models (Irikura and Miyake 2001, 2011). The lower limit of the period range of these simulations was 3 s, as determined by the resolution of both the velocity structure model and the source model.

The characterized source model, which consists of multiple asperities and a background area (e.g., Somerville et al. 1999; Miyake et al. 2003), performs well for both short- and long-period ground motions, particularly in reproducing the rupture directivity pulses, as demonstrated in studies on the 1995 Kobe earthquake (e.g., Kamae and Irikura 1998). It is used in the broadband ground motion prediction scheme (called the "recipe") by the Earthquake Research Committee (ERC) of the Headquarters for Earthquake Research Promotion of Japan (ERC 2009; Fujiwara et al. 2009). In the recipe, the long- and short-period components of the ground motion are computed using the 3D finite-difference method (FDM) and the stochastic Green's function method, respectively. The performance of the recipe has been validated mainly for crustal earthquakes with moment magnitudes 6–7 (e.g., Morikawa et al. 2011; Iwaki et al. 2016).

However, the recipe may not be valid for megathrust earthquakes with magnitudes 8 and larger because the characterized source model lacks heterogeneity smaller than asperities, which may not be negligible in simulating ground motion for engineering purposes. Because the characterized source model generates ground motion at periods longer than the corner period $T_C$ of the asperities, ground motion at periods shorter than $T_C$ may not be sufficiently evaluated when combined with a deterministic computation method for long-period ground motion simulations, as noted by Sato et al. (2006). $T_C$ is approximately 10 s for $M_W$ 8 earthquakes and 2–3 s for $M_W$ 7 earthquakes. The deterministic computation method should be used in the period range at which the 3D velocity structure model is valid, which is usually 1–3 s and longer in Japan, and thus, the crossover period $T_{cross}$ at which the deterministic and stochastic methods are matched is usually approximately 1–3 s. Because the source model lacks heterogeneity with corresponding periods shorter than $T_C$, ground motion tends to be underestimated in the period range between $T_C$ and $T_{cross}$ for $M_W$ 8 earthquakes. Therefore, heterogeneities that are smaller than the asperities should be included in the characterized source model to account for the ground motion at periods shorter than $T_C$ of the asperities.

To overcome this issue, Sekiguchi and Yoshimi (2006) proposed a source model with multi-scale heterogeneity, which was applied to the ground motion prediction of future megathrust earthquakes at the Nankai Trough (Sekiguchi et al. 2008). They considered multi-scale spatial heterogeneity to the spatial distributions of two source parameters, the slip and rupture velocity, on the fault. The resultant source model agrees with the omega-square model of the source spectra and the slip spectra model by Mai and Beroza (2002). Spatial heterogeneities in the slip and rupture velocity are theoretically necessary for the omega-square model as presented by Hisada (2001).

The aim of this study is to validate a method for generating ground motion for megathrust earthquakes in the period range of approximately 2 s and longer by using the characterized source model combined with multi-scale spatial heterogeneity. Source models are constructed for the 2003 $M_W$ 8.3 Tokachi-oki earthquake, which occurred off the southeastern coast of Hokkaido, Japan, at the Kuril Trench. Long-period ground motion simulations are then conducted using a 3D FDM with the source model and a 3D velocity structure model, and their performance was tested by comparing the simulated ground motion with the observed records. The effects of heterogeneity of each source parameter on the predicted ground motion are revealed by comparing the heterogeneous models with the characterized models without heterogeneity. In addition, we refer to a slip-inversion model to examine which parameter's heterogeneity is the most important for reproducing the complicated observed ground motion.

## Source models

Figure 1 shows a schematic of the eight types of source models used in this study. Model 0 is the slip model by Aoi et al. (2008) obtained from waveform inversion analysis, which is used as a reference in this study. Model C is the characterized source model derived from Model 0 following the recipe, as described in "Model C: Characterized source model." Models H1, H2, and H3 are hereafter referred to as the heterogeneous models, and they contain heterogeneous spatial distribution of one or more of the following three parameters: slip, rupture velocity, and rake angle. First, multi-scale heterogeneity is added to the spatial distribution of slip in Model C to yield Model H1. Then, multi-scale heterogeneity is added to the spatial distribution of the rupture velocity of Model H1 to yield Model H2. Finally, Model H3 contains a heterogeneous distribution of the rake angle, in addition to the heterogeneous slip and rupture velocity distributions found in Model H2. Models H1, H2, and H3 are described in more detail in "Models H1–H3: Heterogeneous source models." Conversely, Models S1, S2, and S3 are called the simplified models, and they are derived

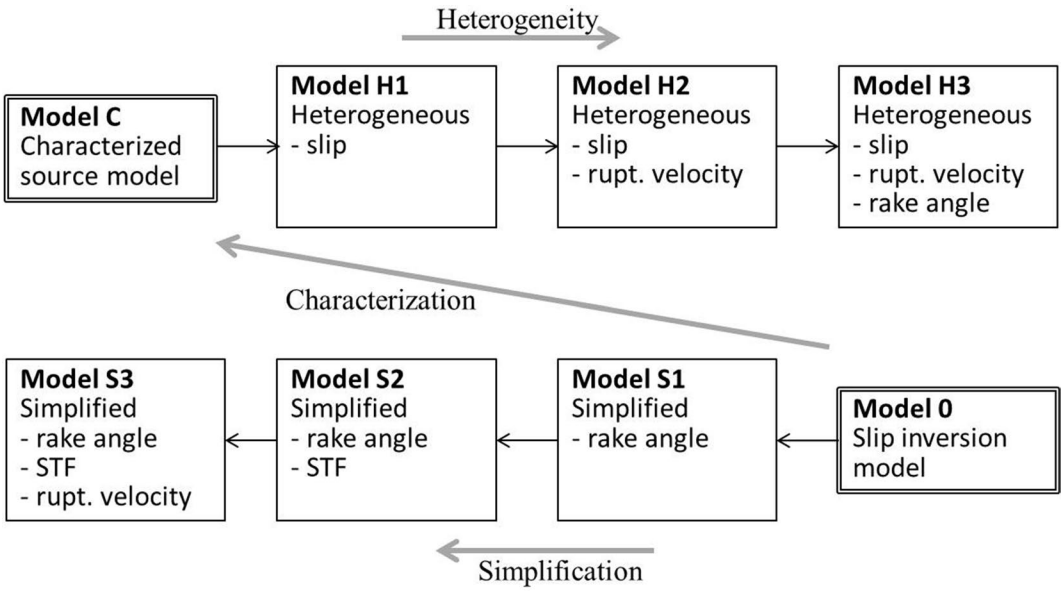


**Fig. 1** Schematic of the source models considered in this study. The heterogeneous Models H1–H3 are generated by cumulatively adding heterogeneity to the parameters of Model C. The simplified Models S1–S3 are generated by cumulatively simplifying the parameters of Model 0. STF stands for source time function

from simplifications of Model 0, as described in "Models S1–S3: Simplified source models." The spatial distributions of the rake angle, the shapes of slip velocity function (SVF), and the rupture velocity are simplified in sequence to obtain Models S1, S2, and S3.

#### Model 0: Inversion model (reference model)

Figure 2 shows a map of the study area and the locations of 15 stations of the strong motion seismograph networks K-NET and KiK-net (Aoi et al. 2011) of the National Research Institute for Earth Science and Disaster Prevention (NIED). Ground motion data recorded at these stations were used in the waveform inversion analysis by Aoi et al. (2008). The fault location of Model 0, i.e., the slip model by Aoi et al. (2008), is also shown in Fig. 2. Model 0 is composed of 460 subfaults, each of which has a size of 7 km × 7 km (length × width). Each subfault is further divided into 5 × 5 point sources for use in FDM computation, yielding a total of 11,500 point sources. The 25 point sources within each subfault have the same source parameters except for the rupture time, which reflects the rupture propagation effect. The SVFs of the subfaults are represented by smoothed ramp functions with 10 time windows of 2.5 s in duration separated by 1.25 s. The first time window propagates at a constant velocity of 3.9 km/s. The rake angles vary spatially and temporally within 127° ± 45°. The distribution of the total moment release is shown in Fig. 3, in which each square—block represents a subfault.

#### Model C: Characterized source model

Model C is constructed by characterizing the kinematic parameters of Model 0. The characterized source model is represented by the parameters listed in Table 1 (e.g., Irikura and Miyake 2011). The basic procedure of the recipe (ERC 2009) was employed to determine the parameters. Several parameters (the total area of the asperities $S_a$, the area $S_{ai}$ and stress drop $\Delta\sigma_{ai}$ of each asperity, and the rupture velocity $V_R$) are estimated by a trial-and-error approach; that is, we searched for suitable parameters that well describe the observed ground motion in a period range of approximately 5–10 s, which is particularly dominant in the observations at many stations, by conducting 3D simulations using several values for each parameter.

The fault configuration, the fault area $S$, and the seismic moment $M_0$ of Model C are taken from Model 0. The average stress drop $\Delta\sigma$ is set to 3.2 MPa, based on the circular crack model of Eshelby (1957), in which $\Delta\sigma = (7/16) \cdot M_0/R^3$ where $R$ is the radius of the circular fault. Although the Tokachi-oki earthquake is too large to assume a circular fault, this average stress drop was adopted because it is close to the value of 3.0 MPa proposed by Allman and Shearer (2009). The average slip $D$ is given by $D = M_0/(\mu S)$, where the rigidity $\mu$ is set to $6.48 \times 10^{10}$ N/m$^2$.

After preliminary analysis by trial and error, three rectangles that approximately cover the areas with large moment release in Model 0 are defined as the

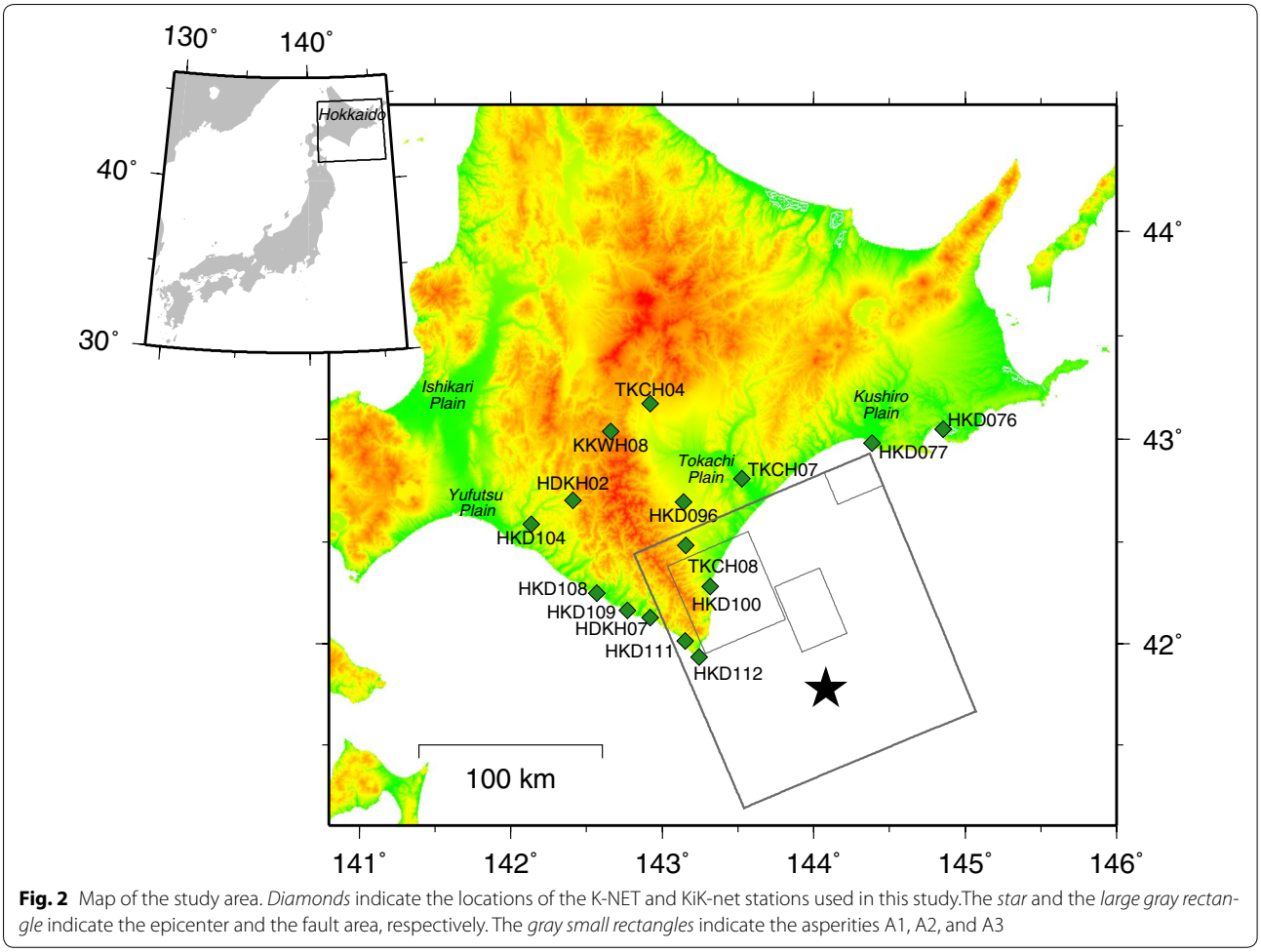


**Fig. 2** Map of the study area. *Diamonds* indicate the locations of the K-NET and KiK-net stations used in this study.The *star* and the *large gray rectangle* indicate the epicenter and the fault area, respectively. The *gray small rectangles* indicate the asperities A1, A2, and A3

asperities A1, A2, and A3 (gray rectangles in Fig. 3), and the remaining area is defined as the background area (BA). The strong motion generation area (SMGA) models of Kamae and Kawabe (2004) and Morikawa et al. (2006) are also referred to determine the approximate locations of the asperities. The total area of the asperities $S_a$ is set to 20 % of the fault area $S$. In the recipe, the average stress drop of the asperities is given by $\Delta\sigma_a = (S/S_a)\Delta\sigma$ (Madariaga 1979), which is 16 MPa in this case. On the other hand, both Kamae and Kawabe (2004) and Morikawa et al. (2006) suggested relatively high stress drops (25–50 MPa) in the asperities. Therefore, using $\Delta\sigma_a$ as a baseline, several values of the stress drop are considered for each asperity using $\Delta\sigma_{ai} = \alpha_i \times \Delta\sigma_a$, with $\alpha_i = 1, 1.5, 2, 2.5, 3$, where $i = 1$, 2, 3 correspond to the asperity number. The average slip within each asperity is given by $D_{ai} = \left(\gamma_j / \sum_J \gamma_j\right) \cdot \xi D$, where $\gamma_i \equiv \sqrt{S_{ai}/S}$ and $\xi = 2.2$ (Somerville et al. 1999).

Two values are considered for the rupture velocity: $V_R = 0.72\, V_s$ and $0.8\, V_s$, where $V_s = 4500$ m/s. We consider multi-hypocenter; that is, when the rupture front reaches a point within an asperity, the rupture is assumed to propagate within the asperity from that point with the same rupture velocity but with new wave fronts. The rake angle is set to constant 127° at all subfaults. The most suitable parameters for Model C are listed in Table 2. The SVF is expressed using the model by Nakamura and Miyatake (2000), which is an approximate expression of slip velocity based on the numerical solutions of 2D and 3D crack models with a slip-weakening friction law (see "Appendix").

### Models H1–H3: Heterogeneous source models

To construct the heterogeneous source models (Models H1, H2, and H3), multi-scale heterogeneity was cumulatively added to the spatial distributions of the slip $D$, rupture velocity $V_R$, and rake angle $\lambda$, using Model C as the initial model. Seven scales of heterogeneity were considered using circular patches with different radii. At each scale ($k = 1, 2, \ldots, 7$), $n_k$ circular patches with radii of $r_k$ are distributed randomly on the fault. The radius of the largest patches ($k = 1$) is chosen such that their area was nearly equal to that of the smallest asperity A3, i.e.,

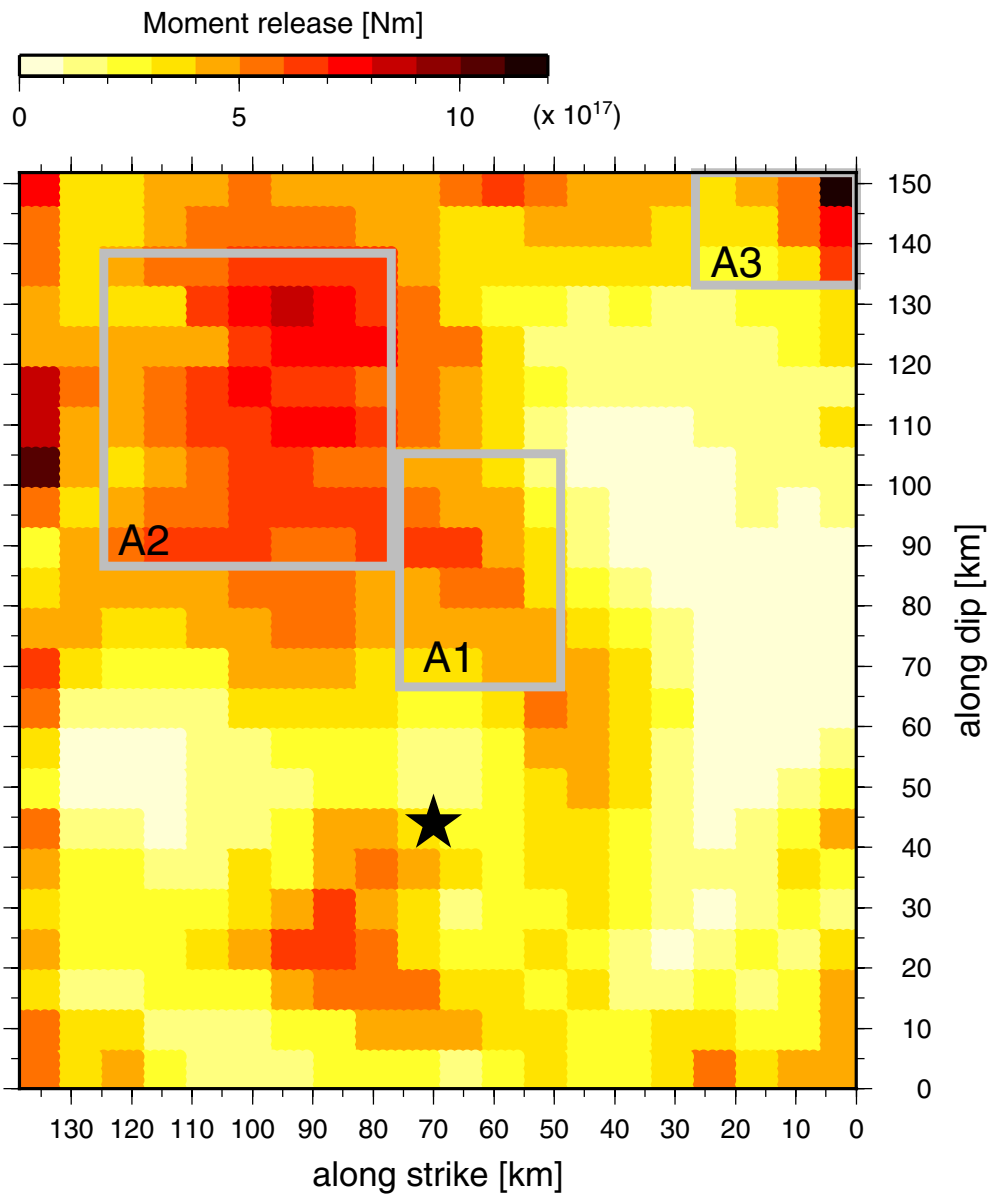


**Fig. 3** Distribution of total moment release of Model 0. *Each colored square* represents a subfault, and each subfault is further divided into 25 point sources. The *star* indicates the rupture starting point. The *gray rectangles* labeled A1, A2, and A3 are the asperities of Model C

$r_1 \sim \sqrt{S_{a3}/\pi}$. The radius at the $(k+1)$th scale is given by $r_{k+1} = r_k/a$ where the constant $a$ is set to 1.5. The total area of the patches at each scale is constant and almost equal to the total area of the asperities.

At each scale, each point source is judged based on whether it is located inside any of the $n_k$ patches. Three parameters (slip, rupture velocity, and rake angle) of each point source are increased or decreased by a given amount $\Delta p_k$, as

$$p = p_0 + \sum_{k=1}^{7} \Delta p_k \tag{1}$$

where $p$ and $p_0$ are the final and initial values of each parameter, respectively. If a point source is found to be outside all of the patches, then $\Delta p_k = 0$; otherwise, the value of $\Delta p_K$ is randomly determined within the range of variation, or fluctuation, for each parameter, as listed in Table 3; these ranges determine the strength of the heterogeneity. The range of rake angle follows in the inversion analysis of Aoi et al. (2008). The rake angles were allowed to vary within ±45° of 127°, which is the focal mechanism solution by F-net (Okada et al. 2004; http://www.fnet.bosai.go.jp/top.php?LANG=en). The fluctuation of the slip is proportional to the patch radius (Sekiguchi et al.

**Table 1 Source parameters considered in the characterized source model**

| Outer source parameter | Inner source parameter | Others |
|---|---|---|
| Fault configuration# | Total area of asperities $S_a$* | Slip velocity function |
| Fault area $S$# | *Asperities* | Rupture velocity $V_R$* |
| Seismic moment $M_0$# | Area $S_{ai}$* | Rake angle |
| Average stress drop $\Delta\sigma$ | Stress drop $\Delta\sigma_{ai}$* | |
| Average slip $D$ | Average slip $D_{ai}$ | |
| | *Background area* | |
| | Area $S_b$ | |
| | Stress drop $\Delta\sigma_b$ | |
| | Average slip $D_b$ | |

In this study, the parameters with # are given by Model 0. The parameters with * are estimated by a trial-and-error approach. The remaining parameters are obtained by following the recipe

2008). The fluctuations for the slip and rupture velocity are determined by fitting the source spectra with $\omega^{-2}$ model and the wavenumber slip spectra with $k^{-2}$ decay at high wave numbers. The final value of $V_R$ is constrained to be nonnegative and less than 120 % of the shear-wave velocity. Supershear and near-supershear ruptures have been reported by several studies (e.g., Yagi 2004; Koketsu et al. 2004). On average, approximately 98 % of 11,500 subfaults remained subshear rupture. The moment rate function, source spectra, and slip spectra of Models 0, C, and H2 are shown in Fig. 4.

The same spatial distributions in the patches are used for the slip and rupture velocity. Therefore, the rupture velocity is assumed to increase when the slip increases. This is similar in principle to other source models for ground motion prediction (e.g., Frankel 2009; Graves and Pitarka 2010), in which a positive correlation between slip and rupture velocity is assumed. This assumption is consistent with several dynamic rupture models (e.g., Day 1982; Song and Somerville 2010), whereas Schmedes et al. (2010, 2013) reported that such correlation is unclear at least under certain conditions of dynamic rupture models. Therefore, it should be noted that it remains unclear whether this assumption is appropriate.

**Table 2 Source parameters for Model C**

| Area $S$ (km$^2$) | Seismic moment $M_0$ (Nm) | Average slip $D$ (m) | Average stress drop $\Delta\sigma$ (MPa) | Rupture velocity $V_R$ (m/s) | |
|---|---|---|---|---|---|
| 21,038 | 3.98E + 21 | 2.92 | 3.18 | 3600 | |
| **Asperities** | **Area $S_{ai}$ (km$^2$)** | **Seismic moment $M_0$ (Nm)** | **Average slip $D_{ai}$, $D_b$ (m)** | **Average stress drop $\Delta\sigma_{ai}$, $\Delta\sigma_b$ (MPa)** | **$\alpha_i$** |
| A1 | 1098 | 3.56E+20 | 5.01 | 16.0 | 1 |
| A2 | 2561 | 1.27E+21 | 7.65 | 32.0 | 2 |
| A3 | 549 | 1.26E+20 | 3.54 | 40.0 | 2.5 |
| BA | 16,381 | 2.23E+21 | 2.04 | 1.48 | |

### Models S1–S3: Simplified source models

Watanabe et al. (2008) studied the complexity of the source model for the 2003 Tokachi-oki earthquake by Honda et al. (2004) by simplifying the source parameters, with the objective of extracting the dominant parameters that strongly influence the resulting ground motion. In this study, Models S1, S2, and S3 were constructed by simplifying the spatial heterogeneities of the source parameters of Model 0 in a manner similar way to the method in Watanabe et al. (2008). Model S1 has a uniform rake angle (127°) in all subfaults during all time windows. Model S2 has a uniform SVF shape for all subfaults, in addition to a uniform rake angle. Figure 5 shows the SVF of each subfault for Models S1 and S2 (the SVFs of Model S1 are the same as those of Model 0). Among the various SVFs of the subfaults of Model S1, one with a Kostrov-type shape (bold square in Fig. 5) is selected. Then, all SVFs of Model S2 are set to have the same shape as the selected Kostrov-type SVF, with the seismic moment and time $t_{\mathrm{peak}}$ when the SVF reaches the peak value defined as the same as those for the corresponding subfault in Model S1. Model S3 has a uniformly distributed rupture velocity $V_{\mathrm{R}} = 3600$ m/s over the fault, in addition to a uniform rake angle and SVF shape. Therefore, $t_{\mathrm{peak}}$ and the rupture front have circular distributions in Model S3.

The spatial distributions of the rake angle, rupture time, and slip of Models 0, C, S1–S3, and H1–H3 are shown in Fig. 6. Because the rake angle of Model 0 varies temporally in the multiple time window representation, the rake angle of the time window with the largest slip velocity is plotted. Similarly, the plotted rupture times of Models 0, S1, and S2 represent the beginning of the time window in which $t_{\mathrm{peak}}$ takes place.

## Ground motion simulation

Ground motion is computed using the 3D FDM with discontinuous grids (Aoi and Fujiwara 1999) on the open-source software GMS (Aoi et al. 2004) using the source models described in the previous section and the 3D layered velocity structure model by Aoi et al. (2008). The velocity structure model covers the upper mantle, the crust, and the Quaternary to Late Cretaceous sedimentary layers, the physical parameters of which are listed in Table 4. The smallest S-wave velocity considered in the model is 500 m/s, which is considered to be the S-wave velocity of the engineering bedrock. The grid size is set to 150 m × 75 m (horizontal × vertical) in the shallow region (depth <10 km). Because the FDM

**Table 3 Fluctuation of the parameters for the heterogeneous models**

| | Slip (m) | Rupture velocity (m/s) | Rake angle |
|---|---|---|---|
| Model H1 | $\pm 0.5D/(a^{k-1})$ | – | – |
| Model H2 | | ±400 | – |
| Model H3 | | | ±45° |

*D* is the average slip of the entire fault, and the constant *a* is set to 1.5 at scale *k*

code implements discontinuous grids to reduce the computational cost, the grid size is three times larger in the deeper region than in the shallower region.

In the following section, the simulated and observed ground motions at a total of 15 K-NET and KiK-net stations (locations indicated in Fig. 2) are examined after band-pass filtering between 0.05 and 0.5 Hz. KiK-net stations have sensors on the ground surface and in boreholes, but only the borehole records are used in this study. The K-NET stations used in this study are located on relatively stiff site conditions, where the effects of nonlinear site responses are assumed to be small.

## Results

### Validation of heterogeneous source models

Examples of velocity waveforms of the simulated ground motion for Models 0, C, and H1–H3 are compared with the observed waveforms in Fig. 7. As expected, waveforms for Model 0 show good agreement with the observed waveforms. Model C explains the distinctive long-period (~10 s) phases with large amplitudes;

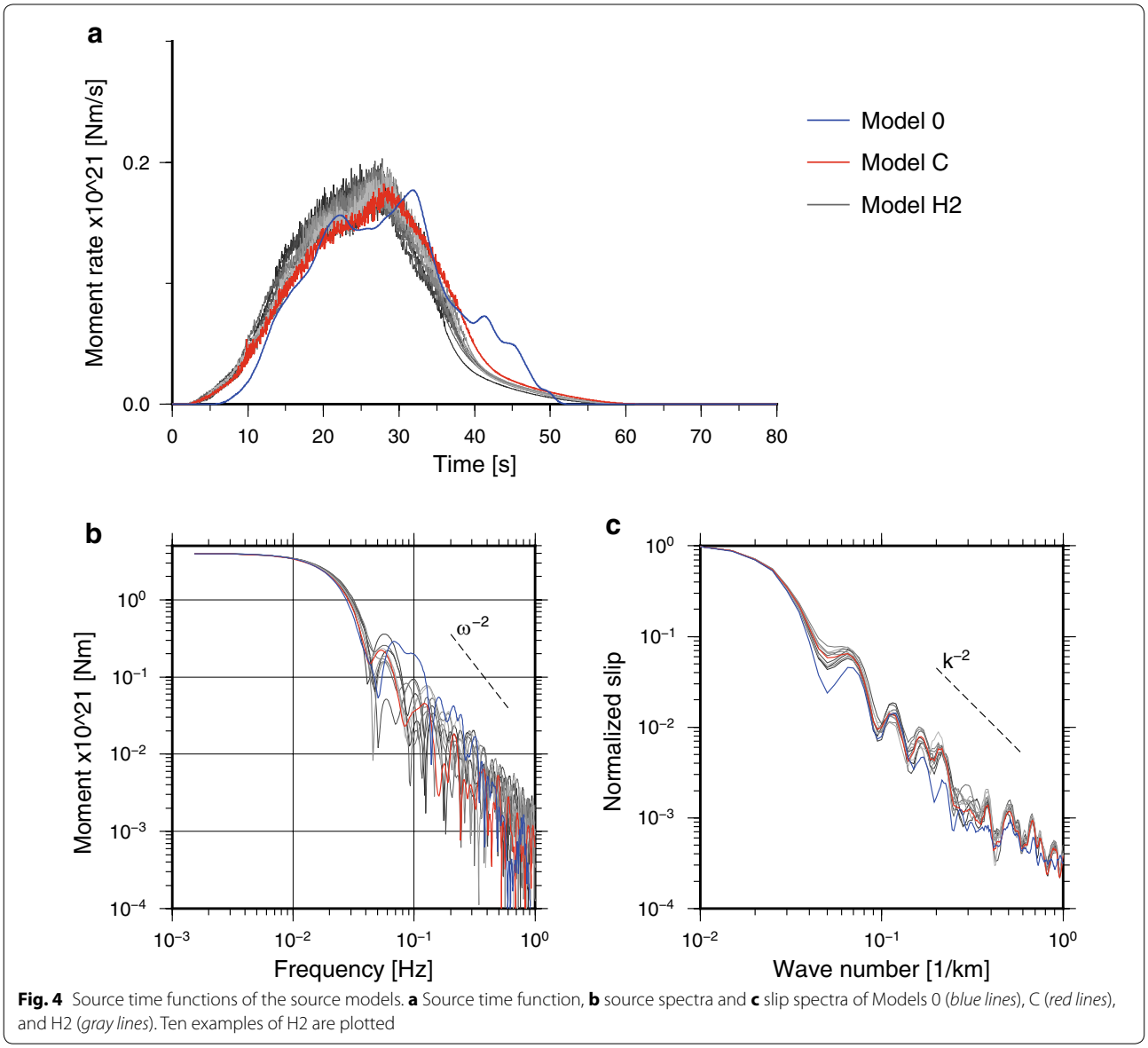


**Fig. 4** Source time functions of the source models. **a** Source time function, **b** source spectra and **c** slip spectra of Models 0 (*blue lines*), C (*red lines*), and H2 (*gray lines*). Ten examples of H2 are plotted

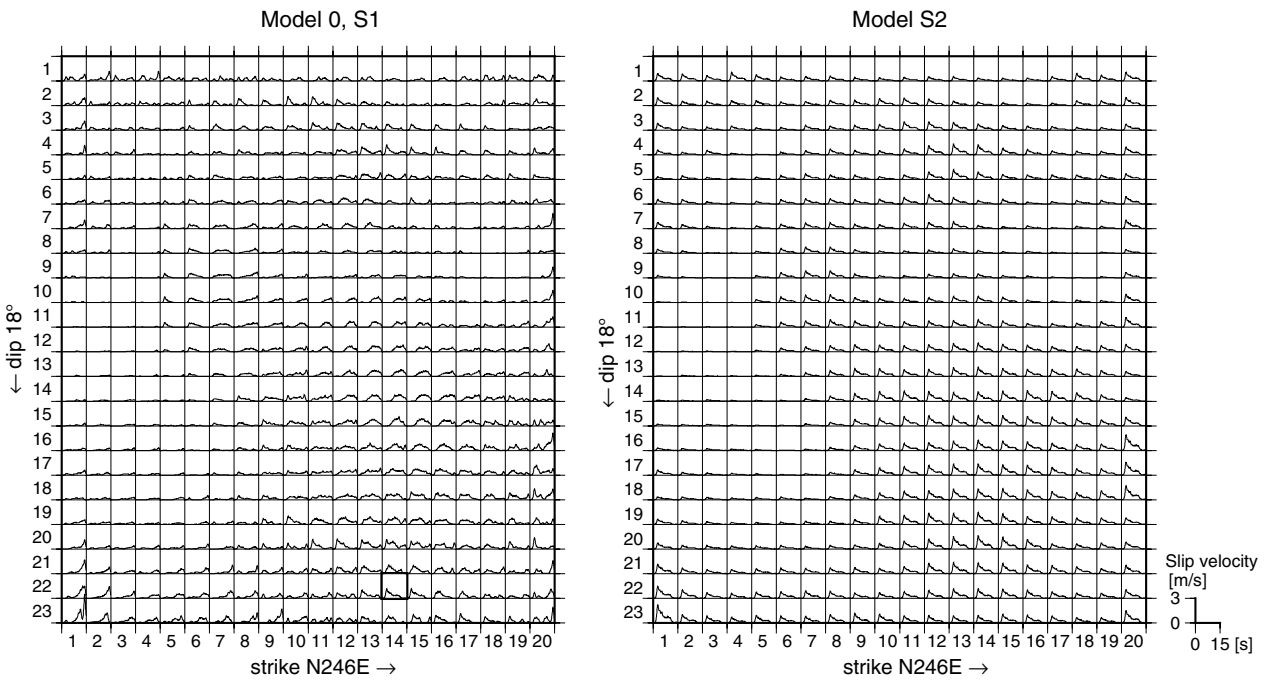


**Fig. 5** Slip velocity functions of Models S1 and S2. The SVFs of Model S1 are the same as that of Model 0, and they vary over the 20 × 23 subfaults. In contrast, all SVFs of Model S2 have a uniform Kostrov-type shape (*the same shape* as the SVF of the subfault indicated by the *bold square* in Model S1)

however, it underestimates shorter-period components. In contrast, Models H1–H3 contain more short-period components than Model C and are more consistent with the observed waveforms.

Fourier amplitude spectral ratios (FASRs) of the simulated ground motion of Models H2 and H3 to that of Model C are plotted in Fig. 8. The mean and standard deviation are taken for the 25 patterns of heterogeneity in each model. We preliminarily calculated the mean and standard deviation of the FASRs of Model H3 using $n = 5$, 10, 15, 20, 25, 30, 35 patterns of heterogeneity and found that the ratio of mean to standard deviation for $n \geq 20$ is within 5 % of that for $n = 35$. Although the FASRs are near 1 at periods of 10 s and longer (<0.1 Hz) for both Models H2 and H3, they are amplified by a factor of 5–10 at the maximum at shorter periods, especially at periods 5 s and shorter (0.2–0.5 Hz). Similarly, FASRs for Models 0, C, and H3 to the observation are plotted in Fig. 9. Although the source parameters are chosen by trial and error to explain the observed ground motion at approximately 5–10 s, Model C still underestimates the observation at many stations, especially at periods of 5 s and shorter. On the other hand, the FASR of Model H3 is closer to 1 than that of Model C at many stations at wide period range (2–20 s).

The FASRs (simulation over observation) of Models 0, C, and H1–H3 averaged over 15 stations are plotted in Fig. 10. The FASRs are also averaged over 10 patterns of heterogeneity for Models H1 and H2 and 25 patterns for Model H3. Because the objective of this study is to obtain an appropriate source model for long-period ground motion prediction and not to precisely reproduce the observed waveforms at each site, the averaged FASR is regarded as a robust index of the performance of the source models. The averaged FASR of Model 0 is near 1 except at periods shorter than 3 s, which is outside the target range of the inversion (Aoi et al. 2008), whereas that for Model C is close to 1 at periods of 10 s and longer (<0.1 Hz) but largely underestimates the observations at shorter periods (>0.1 Hz). This underestimation is caused by the asperity size in Model C as mentioned in the introduction. The asperities are approximately 30–60 km in width and length, which correspond to corner periods $T_C$ of roughly 6–12 s. On the other hand, the averaged FASRs of Models H1–H3 are better than that of Model C. In particular, Model H3 shows substantially better results in the period range of 2–20 s.

The spatial distribution of the 5 % damped velocity response spectra (Sv) at periods of 2, 3, 5, 7, and 10 s for Models 0, C, and H3 (averaged over 25 models) is plotted

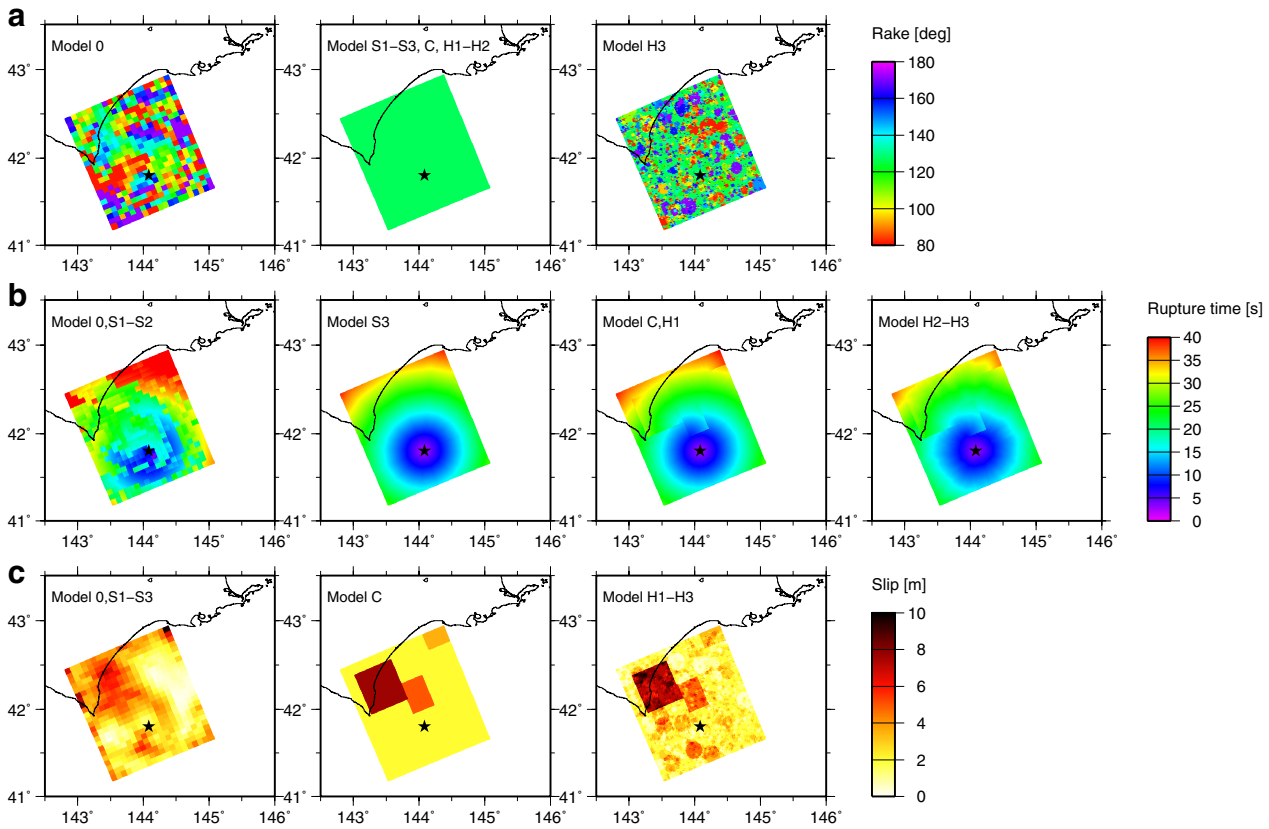


**Fig. 6** Distributions of source parameters. **a** Rake angle, **b** rupture time, and **c** slip of Models 0, *C*, *H1–H3*, and *S1–S3*. For Model 0, the rake angles and rupture time of the time window in which the peak slip velocity occurs are plotted. The rupture time distribution of Models *C* and *H1* differs from that of Model *S3* because they consider multiple hypocenters

**Table 4 Layers of the velocity structure model by Aoi et al. (2008)**

| Layer | $V_P$ (m/s) | $V_S$ (m/s) | $\rho$ (kg/m$^3$) | $Q$ |
|---|---|---|---|---|
| 1 | 1800 | 500 | 1900 | 100 |
| 2 | 2100 | 700 | 2000 | 250 |
| 3 | 2500 | 1100 | 2200 | 1000 |
| 4 | 3300 | 1700 | 2300 | 1000 |
| 5 | 4000 | 2200 | 2450 | 1000 |
| 6[a] | 6000–8200 | 3550–4630 | | |

[a] The parameters of the bottom layer (lower crust and mantle) vary with depth

in Fig. 11. The observed Sv at the K-NET and KiK-net (borehole) stations were computed after applying a band-pass filter at 2–20 s and are plotted on the maps for comparison. It should be noted that the observed Sv at the K-NET stations include the effects of surface layers and may have been affected by nonlinear site response because the data are recorded on the ground surface, although we did not use stations where distinctive nonlinear site responses have been reported by several papers (e.g., Yamanaka et al. 2004; Morikawa et al. 2006). In the southeastern region of Hokkaido, Model H3 generally more closely agrees with the observations than Model C, especially at periods of 2, 3, and 5 s, at which the large values of Sv along the southeastern coast of Hokkaido around Yufutsu, Tokachi, and Kushiro Plains (locations of the plains are shown in Fig. 2) are well reproduced by Model H3. Both Models C and H3 overestimate the observed Sv in the Ishikari Plain in western Hokkaido, whereas Model 0 shows better agreement. All simulations (Models 0, C, and H3) underestimate the observation at several stations in Tokachi and Kushiro plains; the velocity structure model may need to be refined to improve these results.

Figure 12 shows the ratio of Sv of (a) Model H1 to C, (b) Model H2 to H1, and (c) Model H3 to H2 at period 2, 3, 5, 7, and 10 s to illuminate the effect of spatial heterogeneity in the slip, rupture velocity, and rake angle, respectively. Figure 12b indicates that heterogeneity in the rupture velocity increases the Sv by a factor of 1–4 and that its effects are larger at shorter periods. In Fig. 12a, c, the ratio is relatively small compared to that in Fig. 12b,

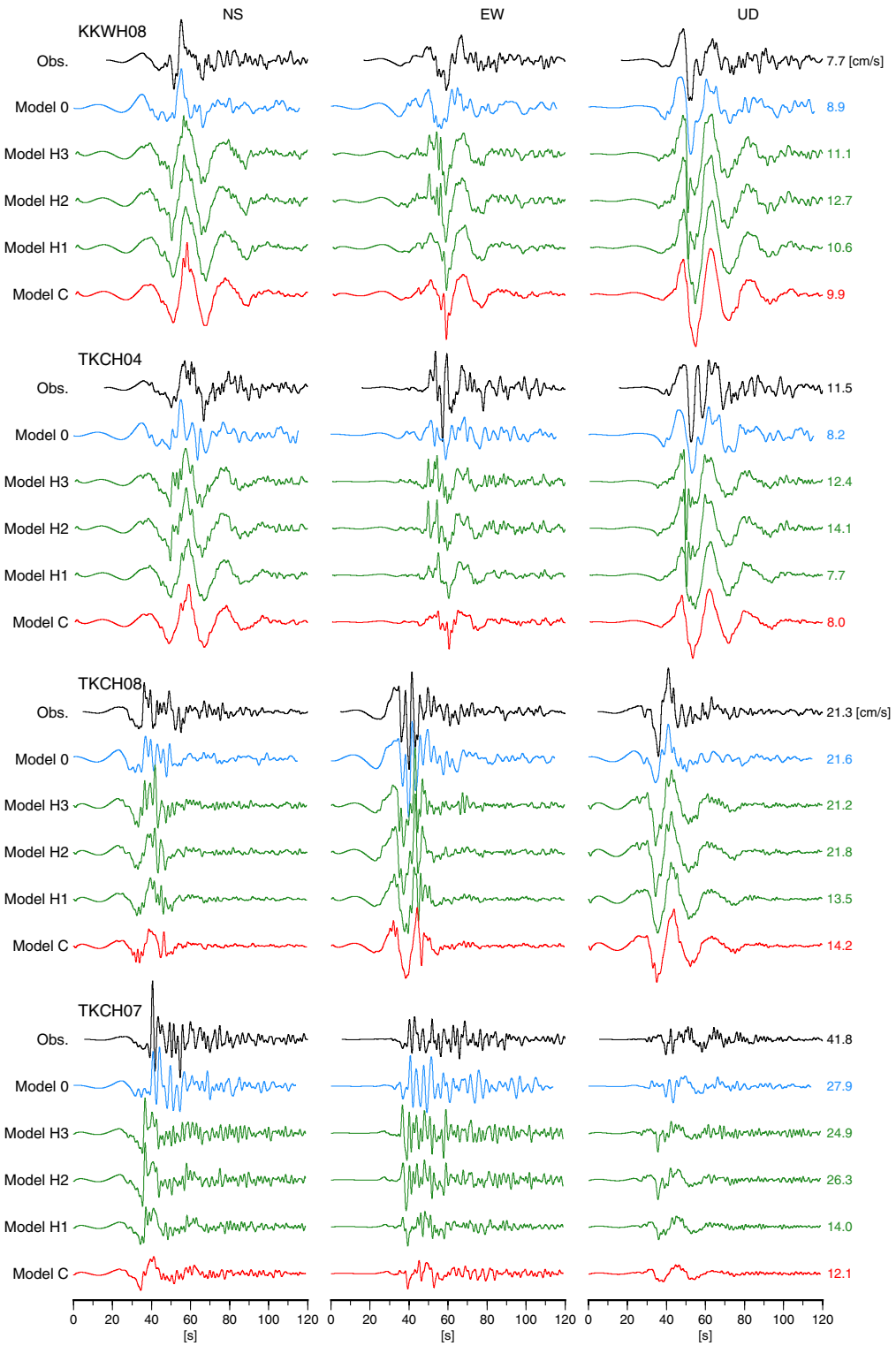


**Fig. 7** Comparison of waveforms. Examples of simulated velocity waveforms for Models 0, C, and H1–H3, compared with observed waveforms. All waveforms are band-pass-filtered between 0.05 and 0.5 Hz

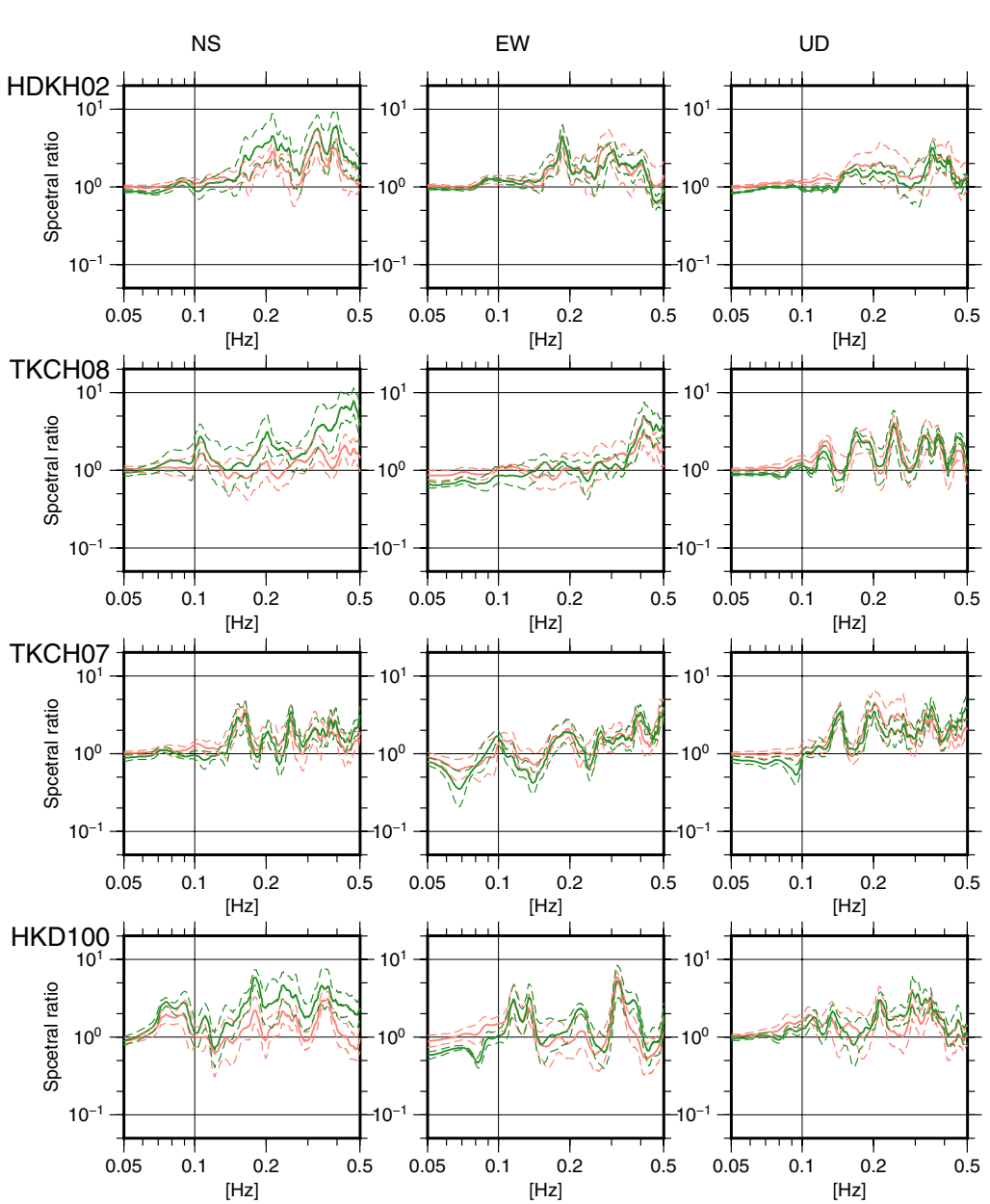


**Fig. 8** Fourier amplitude spectral ratios of Models H2 and H3 to Model C. Ratios are averaged over 10 patterns of heterogeneity of Models H2 and H3. The mean and standard deviation are plotted as *solid* and *dashed lines*, respectively

suggesting that heterogeneity in the slip and rake angle exhibits smaller effects on ground motion compared to heterogeneity in the rupture velocity. However, an area in which the ratio is approximately 2 extends into the central part of Hokkaido at periods of 2 and 3 s. In Fig. 12c, it should be noted that the area in which the ratio is smaller than 1 (blue area) is larger for longer periods. The ERC (2009) noted that uniform rake angle distribution may cause excessive forward directivity effects. Rake angle heterogeneity (Model H3) may have reduced the superposition of radiated waves.

### Effects of simplification

It is clear that among the considered source models in this study, Model 0 best reproduces the observed ground motion, because it contains the complicated rupture process that is needed to explain the observed waveforms. This section attempts to reveal which parameter's

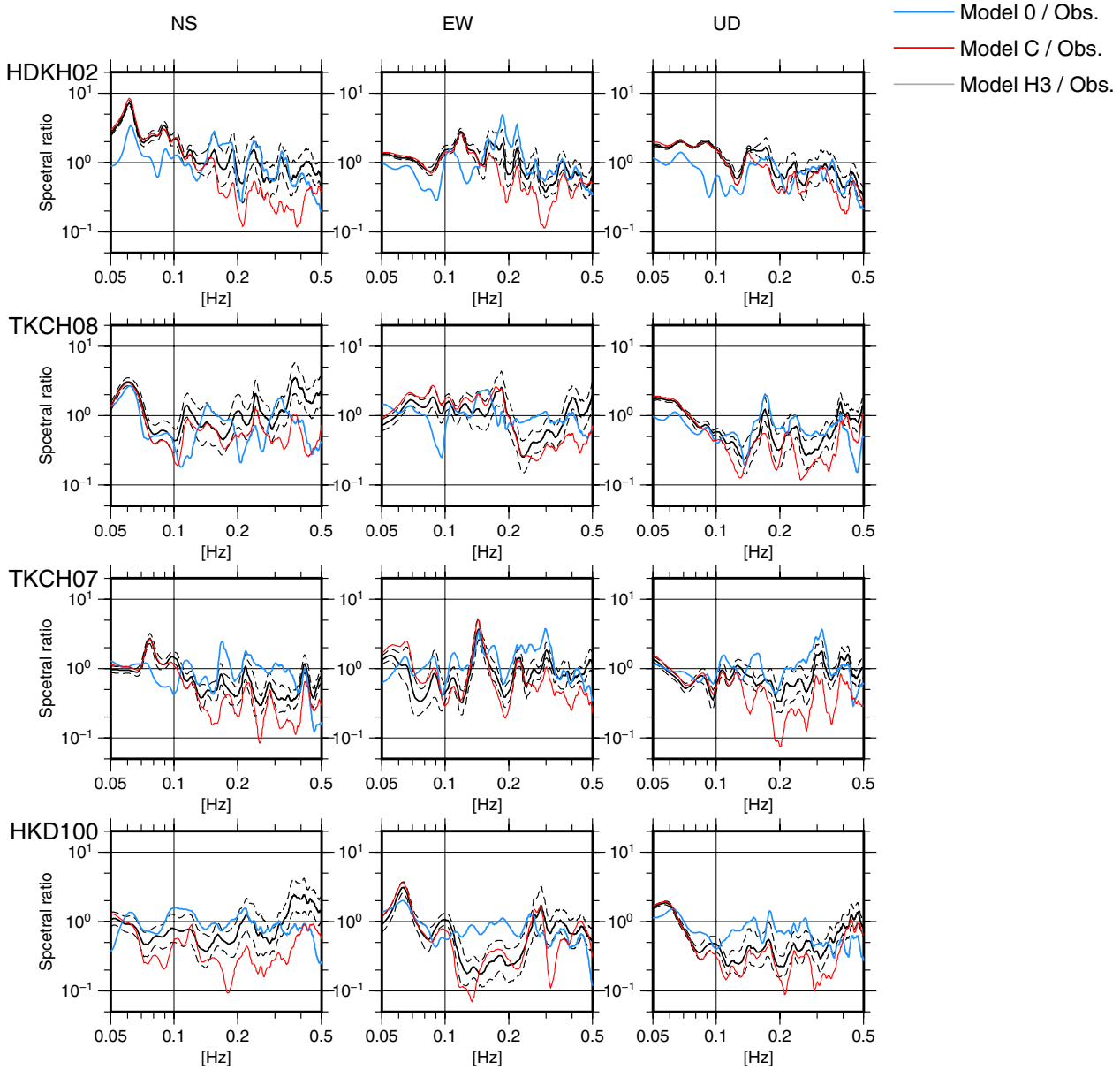


**Fig. 9** Fourier amplitude spectral ratios of Models 0, C, and H3 to the observation. The average is taken over 25 patterns of heterogeneity for Model H3. The mean and standard deviation are plotted as *solid* and *dashed lines*, respectively

heterogeneity is the most crucial for reproducing the observed ground motion, using the simplified Models S1–S3. The averaged FASRs for Models S1–S3 are plotted in Fig. 13. The results in Fig. 13 suggest that simplifying the rupture velocity as in Model S3 has the greatest impact on the performance of the source model, which is consistent with one of the conclusions of Watanabe et al. (2008).

The velocity waveforms of the simulated ground motion for Models 0 and S1–S3 are compared with the observed waveforms in Fig. 14. The largest difference between the waveforms of two sequential models is found between Models S2 and S3. In addition to that, we observe some differences between the waveforms for Models 0 and S1, and Models S1 and S2. For example, the distinctive short-period pulse, which yields a peak ground velocity (PGV)

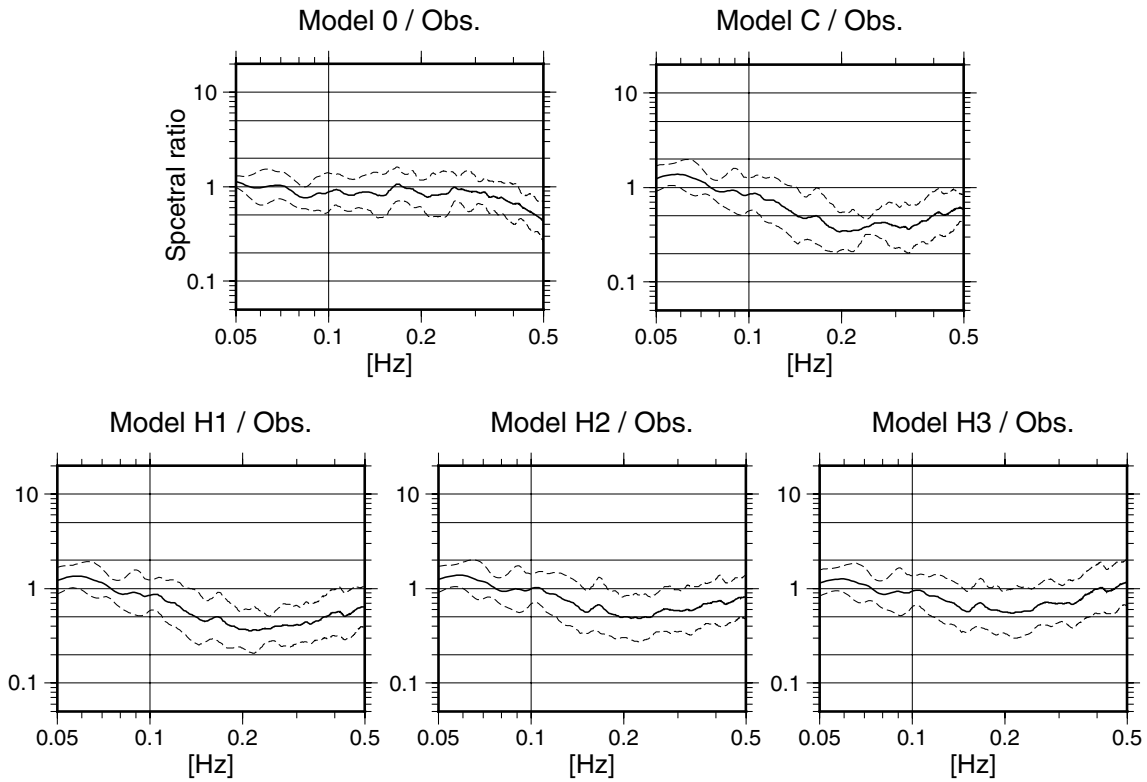


**Fig. 10** Fourier amplitude spectral ratios of the simulations to the observation. The ratios of Models 0, C, and H1–H3 to the observation are averaged over 15 stations. The mean and standard deviation are plotted as *solid* and *dashed lines*, respectively

of approximately 40 cm/s, observed in the NS component at TKCH07 is not reproduced by Model S1, resulting in a PGV of ~20 cm/s, whereas it is reasonably reproduced by Model 0. Similarly, the amplitude in the UD component of Model S2 at KKWH08 is approximately 60 % of that of Model S1. Although the influence of the heterogeneity in the rake angle and SVFs is relatively small on average, it can cause large amplitude or PGV in some situations.

## Discussion and conclusion

This study validated a method for constructing a kinematic source model for ground motion simulations of megathrust earthquakes in the period range of approximately 2 s and longer by combining multi-scale heterogeneity (Sekiguchi and Yoshimi 2006) with the characterized source model. Source models were constructed for the 2003 $M_W$ 8.3 Tokachi-oki earthquake, and ground motion simulations were conducted to study the performance of the source models. In deriving the characterized source model (Model C), some parameters (i.e., the total area of the asperities $S_a$, the area $S_{ai}$ and stress drop $\Delta\sigma_{ai}$ of each asperity, and the rupture velocity $V_R$) were estimated by a trial-and-error approach, deviating somewhat from the recipe. As a result, the stress drops of asperities A2 and A3 were larger by a factor of 2 and 2.5, respectively, than those determined by the recipe. Similarly, the rupture velocity was set to 0.8 $V_S$, which is higher than that indicated by the recipe (0.72 $V_S$). These results suggest that the kinematic characteristics of an individual earthquake may deviate substantially from those indicated by the recipe, although the recipe represents the averaged characteristics of past earthquakes.

Multi-scale heterogeneity was added to the spatial distribution of the slip, rupture velocity, and rake angle of the characterized source model to yield heterogeneous source models (Models H1–H3). By investigating the FASRs of the simulated and observed ground motion, we demonstrated that the heterogeneous Model H3 is able to effectively explain the ground motion at periods

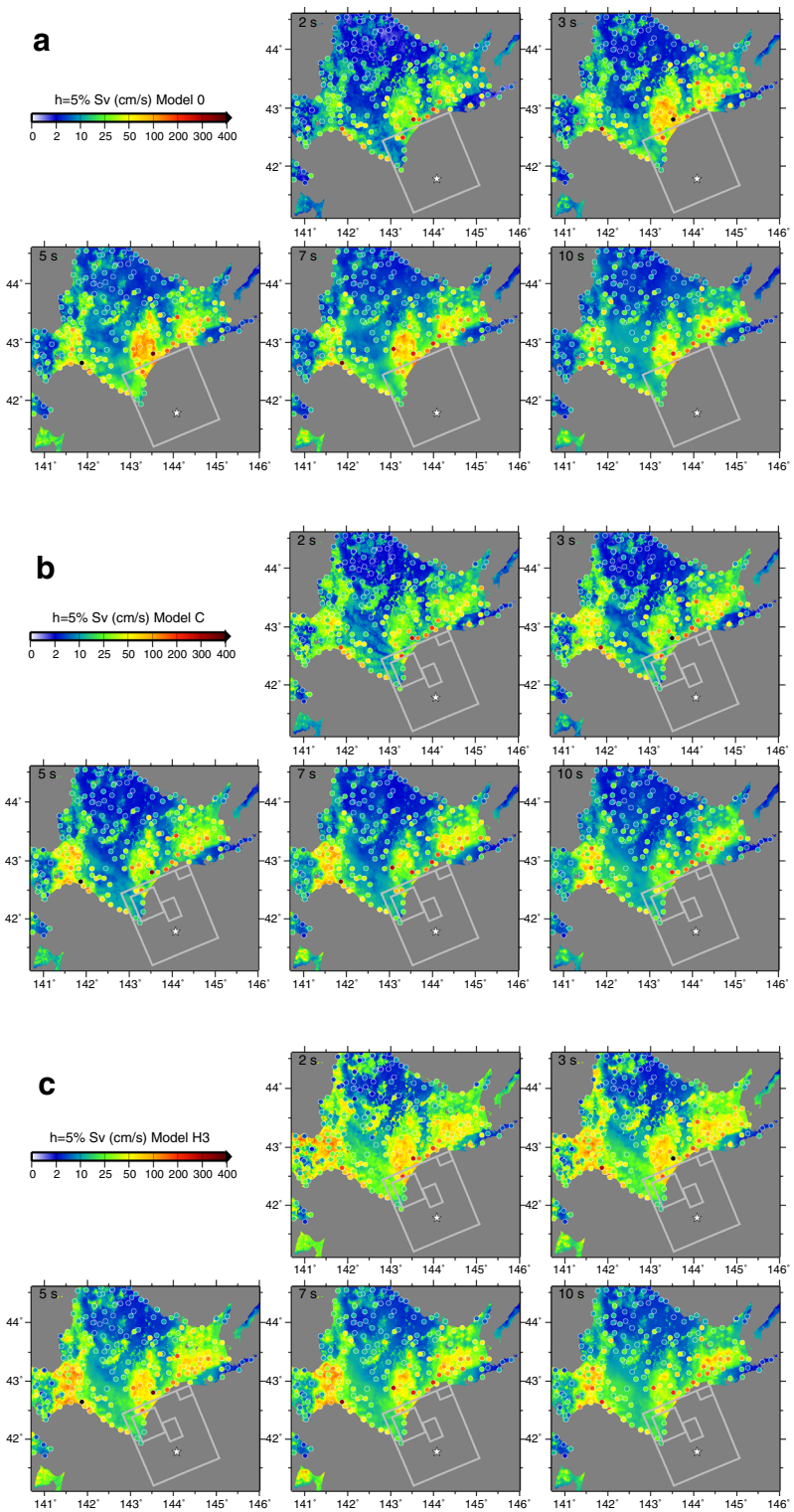


**Fig. 11** Distribution of 5 % damped velocity response spectra (Sv). **a** Model 0, **b** Model C, and **c** Model H3 averaged over 25 heterogeneous patterns at periods of 2, 3, 5, 7, and 10 s. Observed Sv at K-NET and KiK-net stations are plotted with *small circles*. *Gray rectangles* indicate the configurations of the fault and the asperities

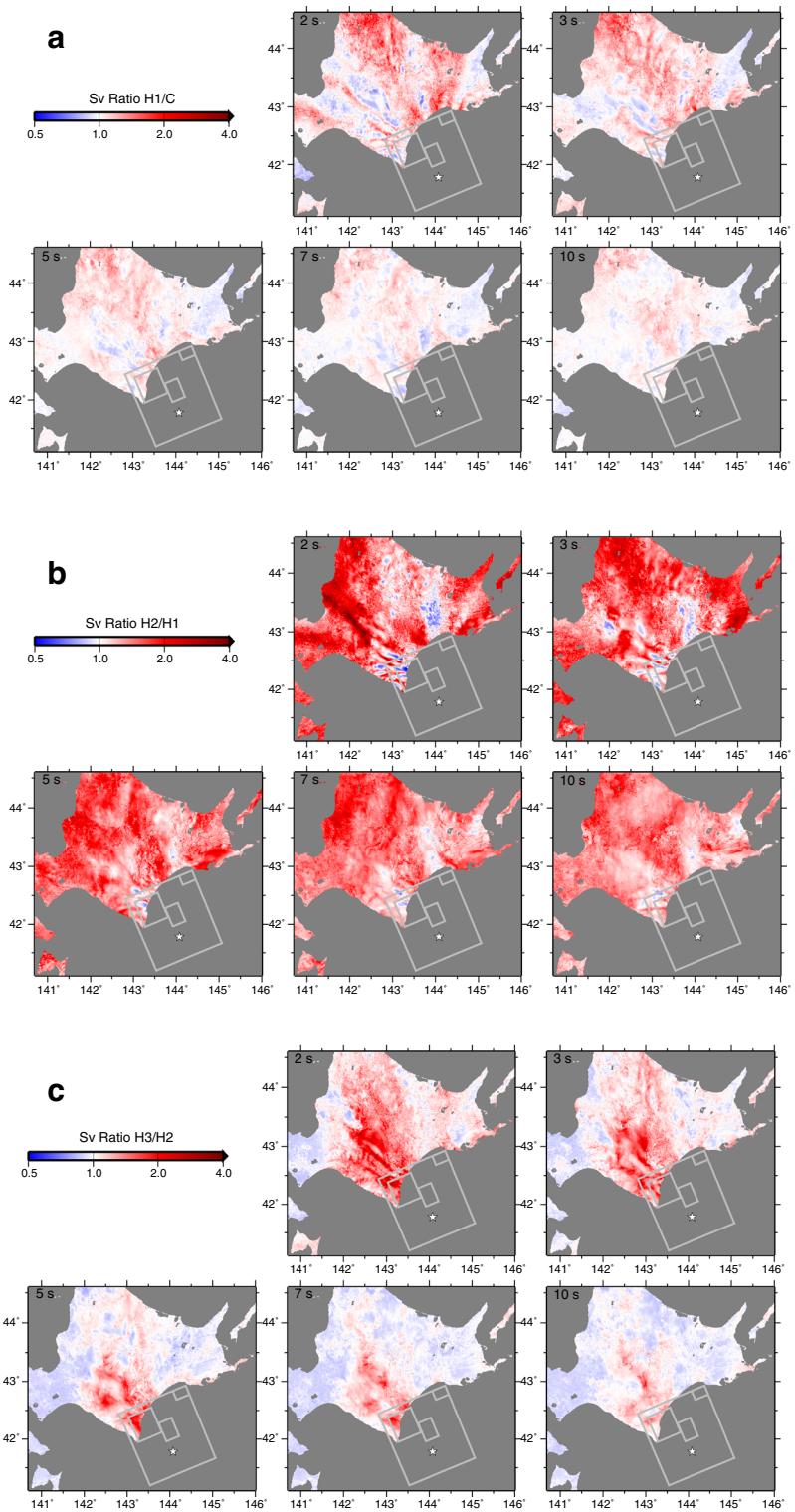


**Fig. 12** Ratio of 5 % damped Sv of different models. **a** Model H1 to Model C. **b** Model H2 to Model H1. **c** Model H3 to Model H2

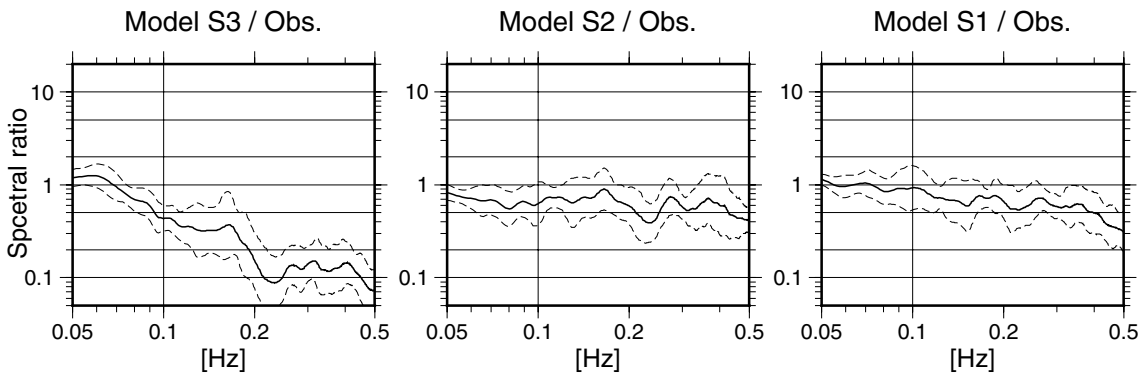


**Fig. 13** Fourier amplitude spectral ratios of the simulations to the observation. Ratios of Models S1–S3 to the observation are averaged over 15 stations. The mean and standard deviation are plotted as *solid* and *dashed lines*, respectively

of 2–20 s. The spatial distribution of the 5 % damped Sv of Model H3 also agreed well with the observation, especially in the southeastern region of Hokkaido. It is suggested that adding multi-scale heterogeneity to the spatial distribution of the slip, rupture velocity, and rake angle of the characterized source model is an effective method for constructing a source model for a future megathrust earthquake that can appropriately generates the ground motion at periods of 2–20 s.

Among the three parameters to which heterogeneity was added, the spatial distribution of the rupture velocity showed the largest influence on the ground motion, which is consistent with Watanabe et al. (2008). We also demonstrated that the distributions of the other two parameters, the slip and rake angle, can also largely alter waveforms and even the PGV. Because it is difficult to precisely model the spatial variation of these parameters, it is important to use a set of source parameters with numerous patterns of heterogeneity.

In this study, source models of a past earthquake were studied. When applying such models to ground motion prediction, it is unrealistic to expect that the precise parameters of the scenario source model can be known before an earthquake occurs because of the complexity of the nature of earthquakes. Therefore, two approaches will be important as future works. One is to comprehend the variability of the source parameters by analyzing the ground motion records of past earthquakes. The other is to introduce probabilistic source models that cover the variability generated by a Monte Carlo sampling method (e.g., Yamada et al. 2011) and perform large amount of ground motion computation.

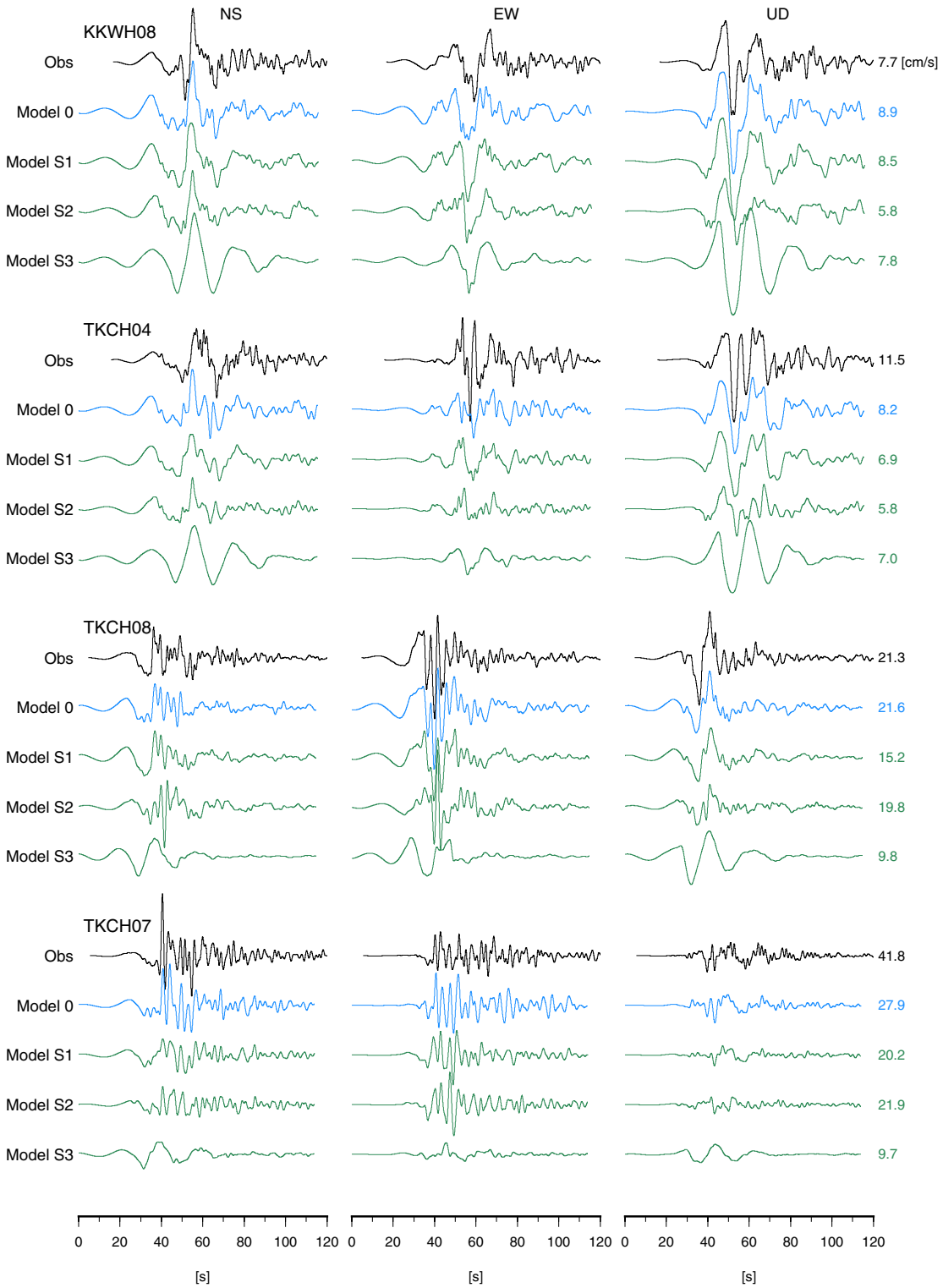


**Fig. 14** Comparison of waveforms. Examples of simulated velocity waveforms for Models 0 and S1–S3, compared with observed waveforms. All waveforms are band-pass-filtered between 0.05 and 0.5 Hz

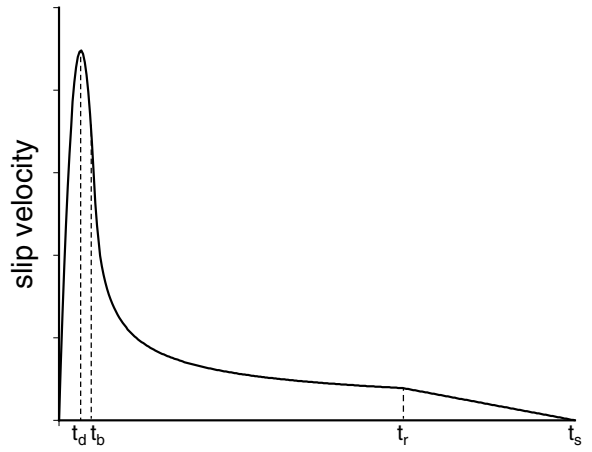


**Fig. 15** Slip velocity function proposed by Nakamura and Miyatake (2000)

**Authors' contributions**
AI conducted the simulations, analyzed the data, and drafted the manuscript. TM, NM, and HF participated in the conception and design of the study and helped interpret the results. SA contributed to constructing the FDM code, the source model (Model 0), and the 3D velocity structure model and helped interpret the results. All authors read and approved the final manuscript.

**Acknowledgements**
Comments from Dr. Kim B. Olsen and an anonymous reviewer helped us improve the manuscript. This study was supported by the "Support Program for Long-period Ground Motion Hazard Maps of Japan" of the Ministry of Education, Culture, Sports, Science, and Technology of Japan. Most figures were drawn using the Generic Mapping Tools software (Wessel and Smith 1998).

**Competing interests**
The authors declare that they have no competing interests.

## Appendix

The slip velocity function $v(t)$ by Nakamura and Miyatake (2000) is given by

$$v(t) = \begin{cases} \left(\frac{V_m}{t_d^2}\right) t(2t_d - t) & 0 < t < t_b \\ \frac{b}{\sqrt{t-\varepsilon}} & t_b < t < t_r \\ c - a_r(t - t_r) & t_r < t < t_s \\ 0 & t < 0 \text{ or } t > t_s \end{cases} \quad (2)$$

$$\varepsilon = (5t_b - 6t_d)/(4 - 4t_d/t_b) \quad (3)$$

$$b = \left(\frac{V_m}{t_d^2}\right) t_b \sqrt{t_b - \varepsilon}(2t_d - t_b) \quad (4)$$

$$c = b/\sqrt{t_r - \varepsilon} \quad (5)$$

$$a_r = c/(t_s - t_r) \quad (6)$$

where $V_m$ is the peak slip velocity, $t_d$ is the time to reach the peak slip velocity, $t_b$ is the time to start decaying at $1/\sqrt{t}$, $t_r$ is the rise time, and $t_s = 1.5t_r$. Figure 15 shows an example of the slip velocity function.

The time to reach the peak slip velocity $t_d$, the rise time $t_d$, and the peak slip velocity $V_m$ are given by

$$t_d = 1/(\pi f_{\max}) \quad (7)$$

$$t_r = \alpha W / V_R \quad (8)$$

$$V_m = \Delta\sigma \sqrt{2 f_c W V_R} \Big/ \mu \quad (9)$$

where $f_{\max}$ is the source-controlled band limitation at high frequencies (e.g., Papageorgiou and Aki 1983), $\Delta\sigma$ and $W$ are the stress drop and width of the asperity or background area, respectively, $V_R$ is the rupture velocity, $\mu$ is the rigidity, and $\alpha = 0.5$. In this study, $f_{\max}$ is set to 13.5 Hz, following the recipe (ERC 2009).

Received: 17 February 2016 Accepted: 16 May 2016
Published online: 01 June 2016

**References**

Allman BP, Shearer PM (2009) Global variations of stress drop for moderate to large earthquakes. J Geophys Res 114:B01310
Anderson JG, Bodin P, Brune JN, Prince J, Singh SK, Quaas R, Onate M (1986) Strong ground motion from the Michoacan, Mexico, earthquake. Science 233:1043–1049
Aoi S, Fujiwara H (1999) 3D finite-difference method using discontinuous grids. Bull Seism Soc Am 89:918–930
Aoi S, Hayakawa T, Fujiwara H (2004) Ground motion simulator: GMS. BUTSURI-TANSA 57:651–666 **(in Japanese with English abstract)**
Aoi S, Honda R, Morikawa N, Sekiguchi H, Suzuki H, Hayakawa Y, Kunugi T, Fujiwara H (2008) Three-dimensional finite difference simulation of long-period ground motions for the 2003 Tokachi-oki, Japan, earthquake. J Geophys Res 113:B07302
Aoi S, Kunugi T, Nakamura H, Fujiwara H (2011) Deployment of new strong motion seismographs of K-NET and KiK-net. In: Akkar S, Gülkan P, van Eck T (eds) Earthquake data in engineering seismology. Geotechnical, geological and earthquake engineering, vol 14. Springer, Dordrecht, pp 167–186
Day SM (1982) Three-dimensional simulation of spontaneous rupture: the effect of nonuniform prestress. Bull Seism Soc Am 72:1881–1902
Earthquake Research Committee (2009) Strong motion prediction method ("Recipe") for earthquake with specified source faults. http://jishin.go.jp/main/chousa/09_yosokuchizu/g_furoku3.pdf (in Japanese). Accessed November 2015
Eshelby JD (1957) The determination of the elastic field of an ellipsoidal inclusion, and related problems. Proc Math Phys Sci 241:376–396
Frankel A (2009) A constant stress-drop model for producing broadband synthetic seismograms: comparison with the Next Generation Attenuation Relations. Bull Seism Soc Am 99:664–680
Fujiwara H, Kawai S, Aoi S, Morikawa N, Senna S, Kudo N, Ooi M, Hao KX, Wakamatsu K, Ishikawa Y, Okumura T, Ishii T, Matsushima S, Hayakawa Y, Toyama N, Narita A (2009) Technical reports on National Seismic Hazard Maps for Japan. Technical Note of the National Res Inst for Earth Science and Disaster Prevention 336
Graves RW, Pitarka A (2010) Broadband ground-motion simulation using a hybrid approach. Bull Seism Soc Am 100:2095–2123

Hisada Y (2001) A theoretical omega-square model considering spatial variation in slip and rupture velocity. Part 2: case for a two-dimensional source model. Bull Seism Soc Am 91:651–666

Honda R, Aoi S, Morikawa N, Sekiguchi H, Kunugi T, Fujiwara H (2004) Ground motion and rupture process of the 2003 Tokachi-oki earthquake obtained from strong motion data of K-NET and KiK-net. Earth Planets Space 56:317–322

Irikura K, Miyake H (2001) Prediction of strong ground motions for scenario earthquakes. J Geography 110:849–875 **(in Japanese with English abstract)**

Irikura K, Miyake H (2011) Recipe for predicting strong ground motion from crustal earthquake scenarios. Pure App Geophys 168:85–104

Iwaki A, Morikawa N, Maeda T, Aoi S, Fujiwara H (2013) Finite-difference simulation of long-period ground motion for the Sagami trough megathrust earthquakes. J Disast Res 8:926–940

Iwaki A, Maeda T, Morikawa N, Miyake H, Fujiwara H (2016) Validation of the recipe for broadband ground motion simulation of Japanese crustal earthquakes. Bull Seism Soc Am (accepted)

Kamae K, Irikura K (1998) Source model of the 1995 Hyogo-ken Nanbu earthquake and simulation of near-source ground motion. Bull Seism Soc Am 88:400–412

Kamae K, Kawabe H (2004) Source model composed of asperities for the 2003 Tokachi-oki, Japan, earthquake (MJMA = 8.0) estimated by the empirical Green's function method. Earth Planets Space 56:323–327

Koketsu K, Hikima K, Miyazaki S, Ide S (2004) Joint inversion of strong motion and geodetic data for the source process of the 2003 Tokachi-oki, Hokkaido, earthquake. Earth Planets Space 56:329–334

Koketsu K, Hatayama K, Furumura T, Ikegami Y, Akiyama S (2005) Damaging long-period ground motions from the 2003 $M_W$ 8.3 Tokachi-oki, Japan, earthquake. Seism Res Lett 76:67–73

Koketsu K, Miyake H, Afnimar Tanaka Y (2009) A proposal for a standard procedure of modeling 3-D velocity structures and its application to the Tokyo metropolitan area, Japan. Tectonophysics 472:290–300

Madariaga R (1979) On the relation between seismic moment and stress drop in the presence of stress and strength heterogeneity. J Geophys Res 84:2243–2250

Maeda T, Morikawa N, Iwaki A, Aoi S, Fujiwara H (2013) Finite-difference simulation of long-period ground motion for the Nankai trough megathrust earthquakes. J Disast Res 8:912–925

Mai PM, Beroza GC (2002) A spatial random field model to characterize complexity in earthquake slip. J Geophys Res. doi:10.1029/2001JB000588

Miyake H, Iwata T, Irikura K (2003) Source characterization for broadband ground-motion simulation: kinematic heterogeneous source model and strong motion generation area. Bull Seism Soc Am 93:2531–2545

Morikawa N, Aoi S, Honda R, Senna S, Hayakawa Y, Fujiwara H (2006) Application of the "Recipe for strong ground motion evaluation" to the 2003 Tokachi-oki, Japan, earthquake. In: 3rd international symposium on the effects of surface geology on seismic motion, paper no. 48, pp 1–8

Morikawa N, Senna S, Hayakawa Y, Fujiwara H (2011) Shaking maps for scenario earthquakes by applying the upgraded version of the strong ground motion prediction method "recipe". Pure appl Geophys 168:645–657

Nakamura H, Miyatake T (2000) An approximate expression of slip velocity time function for simulation of near-field strong ground motion. Zisin 53:1–9 **(in Japanese with English abstract)**

Okada Y, Kasahara K, Hori S, Obara K, Sekiguchi S, Fujiwara H, Yamamoto A (2004) Recent progress of seismic observation networks in Japan—Hi-net, F-net, K-NET and KiK-net. Earth Planets Space 56:xv–xxviii

Olsen KB, Stephenson WJ, Geisselmeyer A (2008) 3D crustal structure and long-period ground motions from a M9.0 megathrust earthquake in the Pacific Northwest region. J Seismol 12:145–159

Papageorgiou A, Aki K (1983) A specific barrier model for the quantitative description of inhomogeneous faulting and the prediction of strong ground motion. I. Description of the model. Bull Seism Soc Am 73:693–722

Pulido N, Aguilar Z, Tavera H, Chlieh M, Calderon D, Sekiguchi T, Nakai S, Yamazaki F (2015) Scenario source models and strong ground motion for future mega-earthquakes: application to Lima, Central Peru. Bull Seism Soc Am 105:368–386

Sato T, Watanabe M, Hayakawa T (2006) Current issue of long-period strong-motion prediction procedure for an M8 earthquake using characterized source model. Chikyu Monthly 55:110–118 **(in Japanese)**

Sato K, Asano K, Iwata T (2012) Long-period ground motion characteristics of the Osaka sedimentary basin during the 2011 Great Tohoku earthquake. In: Proceedings of 15th world conference on earthquake engineering, Lisbon, Portugal, 2012, paper no 4494

Schmedes J, Archuleta RJ, Lavalleé D (2010) Correlation of earthquake source parameters inferred from dynamic rupture simulations. J Geophys Res 115:B03304

Schmedes J, Archuleta RJ, Lavalleé D (2013) A kinematic rupture model generator incorporating spatial interdependency of earthquake source parameters. Geophys J Int 192:1116–1131

Sekiguchi H, Yoshimi M (2006) Multi-scale heterogeneous source model for wide-band ground motion prediction from giant earthquakes along subduction zones. Chikyu Mon 55:103–109 **(in Japanese)**

Sekiguchi H, Yoshimi M, Horikawa H, Yoshida K, Kunimatsu S, Satake K (2008) Prediction of ground motion in the Osaka sedimentary basin associated with the hypothetical Nankai earthquake. J Seismol 12:185–195

Somerville P, Irikura K, Graves R, Sawada S, Wald D, Abrahamson N, Iwasaki Y, Kagawa T, Smith N, Kowada A (1999) Characterizing crustal earthquake slip models for the prediction of strong ground motion. Seism Res Lett 70:59–80

Song SG, Somerville P (2010) Physics-based earthquake source characterization and modeling with geostatistics. Bull Seism Soc Am 100:482–496

Watanabe M, Fujiwara H, Sato T, Ishii T, Hayakawa T (2008) Effects of complexity of fault rupture process on strong ground motions and extraction of the dominant parameters—study on the rupture process of the 2003 Tokachi-oki earthquake. Zisin 60:253–265 **(in Japanese with English abstract)**

Wessel P, Smith WHF (1998) New, improved version of generic mapping tools released. EOS Trans Am Geophys Union 79:579

Yagi Y (2004) Source rupture process of the 2003 Tokachi-oki earthquake determined by joint inversion of teleseismic body wave and strong ground motion data. Earth Planets Space 56:311–316

Yamada M, Senna S, Fujiwara H (2011) Statistical analysis of ground motion estimated on the basis of a recipe for strong-motion prediction: approach to quantitative evaluation of average and standard deviation of ground motion distribution. Pure appl Geophys 168:141–153

Yamanaka H, Motoki K, Etoh K, Murayama M, Komaba N (2004) Observation of aftershocks of the 2003 Tokachi-Oki earthquake for estimation of local site effects. Earth Planets Space 56:335–340